Magnetism in High-Resolution NMR Probe Design. II: HR MAS

F. DAVID DOTY,* GEORGE ENTZMINGER, Y. ANDY YANG

Doty Scientific, Inc., 700 Clemson Rd., Columbia, SC 29229

ABSTRACT: Various issues affecting nuclear magnetic resonance probe resolution are discussed, with emphasis on high-resolution or magic angle spinning (MAS) in this part. Symmetric positioning of chip capacitors at the magic angles addresses the largest B_0 perturbation with ultra-low-inductance decoupling coils, and symmetric spinner drive designs with silicon-nitride coilforms are shown to be extremely beneficial in reducing spinning-, decoupling-, and variable temperature-induced thermal gradients. Other factors discussed include MAS sample cell design, high frequency (HF) coils, centrifugation, shimming, B_1 homogeneity, B_0 stability, and geometric compensation for variable angle spinning resolution. © 1998 John Wiley & Sons, Inc. Concepts Magn Reson 10: 239–260, 1998

KEY WORDS: susceptibility; probes; MAS; thermal gradients; capacitors; coils; VAS; ceramics

INTRODUCTION

In Part I of this two-part article, we looked at some of the basic physics and properties of magnetism as they related to high-resolution (HR) nuclear magnetic resonance (NMR) probe design, both in liquids and in solids, and some of the reasons it is technically difficult to obtain resolution of several parts per billion (ppb). Some methods of measuring susceptibilities and calculating fields produced by various objects were reviewed, and we noted the beneficial attributes of elliptical symmetries and the finite magic angle cylinder. The properties of various materials important to NMR probe construction were presented, and methods of adjusting the susceptibility of adhesives, wire, foil, and dewar alloys were discussed. In Part II, we look more specifically at probe design issues, especially as they relate to HR magic angle spinning (MAS).

There are a number of situations where spinning at the magic angle is required for HR because of inherently broad lines within the sample: polycrystalline or amorphous solids, mixtures of liquids and solids of differing susceptibilities, inhomogeneous and compartmentalized liquids (tissues), and microsamples (*1*, *2*, *3*). While the complete rotational averaging of cylindrically symmetric isotropic magnetic sources at the magic angle helps enormously in achieving HR under MAS, a number of additional factors must be carefully addressed. The relative importance of the various factors on resolution and the difficulty in addressing them depend strongly on probe design and sample. Despite much prior emphasis

Received 31 October 1997; revised and accepted 27 January 1998.

* Correspondence to: F. David Doty. E-mail: david@doty.usa.com.

Concepts in Magnetic Resonance, Vol. 10(4) 239–260 (1998)
 CCC 1043-7347/98/040239-22

on obtaining the highest decoupling strength with solids, we find that in many cases there are at least four factors of greater influence on resolution: acquisition time (which is limited by either sample heating or capacitor heating), spinning speed, thermal gradients, and sample confinement. Magnetic compensation of the sample coil is often comparable to decoupling strength in importance. Obviously, these generalizations depend heavily on the mix of applications being run on the probe. We will look at many of these requirements from a rather general design perspective before looking in more detail at a particular design in the final section.

SAMPLE SPINNING EFFECTS

In 1951, Carr demonstrated more than an order of magnitude improvement in resolution by slowly spinning ($\sim$ 20 Hz) a liquid sample about an axis perpendicular to $\mathbf{B}_0$. The spinning averages out most inhomogeneities in the plane transverse to the spinning axis (*4*), so the spins usually see a mean field approximately equal to that along the sample axis. This is particularly effective in iron-core magnets where, in addition to the magnet's inhomogeneities, the copper rf coils and truncated cylindrical samples generate short-range transverse gradients (which primarily affect line shape) that cannot be shimmed effectively but can be reduced by an order of magnitude by spinning.

When the sample axis is aligned with $\mathbf{B}_0$, as is normally the case for liquids in a superconducting magnet, spinning has no effect on the inhomogeneities from truncated cylinders, as they are independent or azimuthal angle. Moreover, rf coils in modern high-field probes are generally of thin foil and sometimes compensated. Thus, spinning is primarily to average the transverse inhomogeneities from the magnet and the probe-tuning components, which are usually of low order and thus able to be shimmed to under 0.2% of their initial value. However, capacitors, crossover insulators, uncompensated coil leads, and nonuniform adhesive application which are near the sample coil often generate substantial short-range transverse gradients—especially in probes built before about 1992 and in probes designed for extreme temperatures or other special purposes. These near-field perturbations only partly average under rotation.

Barbara illustrated the above situations plus the magic angle cylinder in Figs. 2–4 in a recent article (*5*). Note that the field plot is a smoothly varying (primarily quadratic) function along the axis for cylinders oriented both perpendicular and parallel to $\mathbf{B}_0$, although the former has a minimum and the latter a maximum in the center. However, the perpendicular cylinder shows variations, increasing with radius, as a function of azimuthal angle. [Note the apparent oscillations arise from the method chosen to represent a three-dimensional (3D) data set in a 2D spiral plot.] Under rotation, these variations are largely averaged, leaving an easily correctable function. The parallel cylinder, on the other hand, has no azimuthal dependence and thus shows no improvement from spinning in a uniform external field.

An undesirable effect of spinning, especially in HR liquids, is the creation of spinning sidebands. The primary mechanism is the B_0 inhomogeneity experienced by the spins in their circular path, which modulates the NMR signal at the spinning frequency and produces additional signals on either side of the resonance (*4*). Perfectly stable spinning of a cylinder along the $\mathbf{B}_0$ axis in a perfect probe in a perfect magnet should not produce sidebands. Indeed, they are generally $\sim 0.1\%$ of the resonance amplitude when the spinning rate exceeds the static width at 0.1% of the maximum amplitude, but this may not be adequate, especially with many 2D techniques. Modern finite element analysis (FEA) software makes it rather easy to design high-order axial shims (although their corrective ranges with small samples are quite limited in a wide-bore magnet) that permit nonspinning resolution approaching 1 ppb. With improved shims and improved coil compensation, more and more HR NMR of liquids is being done nonspinning to avoid problems with spinning sidebands.

HR MAS

As noted earlier, when a solid, uniform magnetic cylinder (of any length, with $|\chi| \ll 1$) is aligned at the magic angle, the fields near the ends are also highly nonuniform; but under rotation, the z-component of the field at any point in the cylinder averages exactly to the axial static value, which is the same as for the sphere—$2\chi/3$ inside the cylinder (*5*). Moreover, the z-component of the field produced by any static isotropic magnetic hollow cylinder aligned at the magic angle

averages to zero at all points (except within the material itself) under rotation about its axis.

For an MAS cylindrical sample of length equal to diameter in a rotor of negligible wall thickness with end caps of negligible length in a perfectly shimmed, zero-susceptibility stator, the nonspinning baseline width for a water sample is about 3.5 ppm (mainly from the end edges, where the ellipsoid approximation is worst) (*5*). For protons at 500 MHz, stable spinning at a rate greater than the spectral width (about 2 kHz) would reduce the linewidth to under 1 Hz with excellent line shape as long as turbulence is not induced. The only motion that achieves the desired averaging is perfectly circular motion, and any radial or axial motion from fluid turbulence or container vibration will reduce the accuracy of the averaging and increase linewidth. Faster spinning may give a little additional narrowing unless turbulence is increased. Andrew showed that for many solids, increasing the spinning rate beyond the static linewidth produced additional line-narrowing approximately in proportion to ω_r^{-2}, where ω_r is the rotational rate (*1*). For inhomogeneous samples that include rigid components, moderately fast spinning (4–14 kHz) may be required for effective narrowing of some of the lines, and this may pose sealing, turbulence, or centrifugation difficulties.

Figure 1 illustrates a simple plastic sealing sample cell fitting precisely inside a ceramic sleeve (rotor) that achieves excellent sealing and helps control turbulence in low-viscosity fluids, where the problems are greatest. For positive sealing, the following conditions must be satisfies:

$$Y_3 > Y_2 > Y_1; \rho_2/Y_2 > \rho_1/Y; \text{and } \rho_2 > \rho_4, \quad [1]$$

where Y_1, Y_2, and Y_3 are Young's moduli of the plug, the cell, and the rotor materials, respectively; and ρ_1, ρ_2, and ρ_4 are the densities of the plug, the cell, and the sample, respectively (*6*). In addition, the plug material should be moderately compliant (Y_1 preferably < 2 GPa) and the materials must be devoid of interfering backgrounds and chemically resistant. Only a light press fit of the plug inside the cell is required to achieve vacuum-tight static sealing when the mating surfaces have been precisely machined. As the spinning speed is increased, the centrifugal pressure generated by the expanding plug in the mouth of the cell is greater than the pressure of the fluid, so a positive seal is assured even at the highest speeds if the cell fits precisely within the ceramic rotor so that it cannot stretch away from the plug.

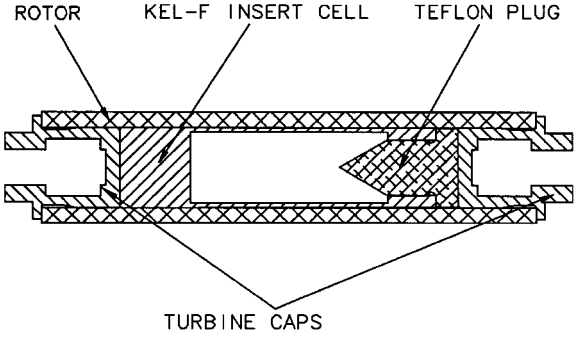

Figure 1 Plastic sealing sample cell inside an MAS rotor with axially symmetric drive turbines.

The conical point on the plug has been found to be effective in suppressing vortex resonances in low-viscosity liquids. Such a geometry results in considerable degradation of NMR line shape for a nonspinning sample if the sample, cell, and plug susceptibilities are not closely matched. However, when spinning at the magic angle, all inhomogeneities from any cylindrically symmetric susceptibility discontinuity, even a point, average to zero. When the point is omitted, vortex resonances can be expected for low-viscosity liquid samples at speeds above 2500 Hz even in highly stable double-bearing spinners. The resonances may be identified by the sudden onset of an additional 5–20 Hz broadening as the speed is increased. This problem does not arise in tissue samples or in combinatorial chemistry (CC) samples, where the swollen resin beads damp fluid resonances.

The materials that usually work best are a kel-f cell and a Teflon plug except where the fluorine or chlorine signal causes problems. The Teflon plugs are usually too loose to seal after operation at high temperatures from small, permanent distortions. For the same reason, they may not seal well at low speeds after high-speed spinning, so they should be considered disposable. In some biological applications, the chemistry is so sensitive to surface reactions that it is necessary to use a Teflon cell with a Teflon plug and accept the reduced spinning speed limits. For fluorine NMR, ultem or aurum is normally chosen for the cell, and the plug is of polyphenylene sulfide (PPS) or polyvinyl chloride (PVC), although both are too hard for effective sealing in many cases. As a last resort, the plug can be epoxied in, which is often required with variable temperature (VT) work.

With an aqueous liquid sample, limited in length to the active coil length, without an air

bubble in a typical kel-f cell, nonspinning baseline widths would be under 0.7 ppm in an ideal stator, as the susceptibility of the cell is a much closer match to the sample than is air, which gave a 3.5-ppm width. Typical variations in bulk magnetic susceptibility (BMS) in CC and within tissues (away from major sample boundaries) are also ~ 0.7 ppm. Thus, spinning above 350 Hz may give adequate line narrowing (at 500 MHz) if the stator and coil can be designed to produce sufficiently low inhomogeneity. Clearly, the rf coils may be compensated, but temperature-independent methods of compensating ceramics have not been developed. We will discuss a satisfactory ceramic stator design in more detail in later, but for now we simply note that a static baseline width (at 0.1% height) of ~ 1.6 ppm may be achieved (and under 0.1 ppm at half-height for water in a kel-f cell. Thus, there is little to be gained from improving the susceptibility match between the cell and the sample, as the stator (at least if designed for solids) will have greater cylindrically symmetric inhomogeneities which set the minimum rotational rate for high resolution at about 800 Hz for protons at 500 MHz. This rate is more than adequate to force any air bubble into a cylindrically symmetric vortex, which has no effect on line shape.

While the above is true for most samples, if the sample cell is almost empty (for example, a 90-μL cell containing < 10 μL of sample), all of the sample is plastered into a thin film against the walls, where the proximity to the rf coil and optics adds some rotationally invariant broadening. This is one reason that a range of sample cell sizes is beneficial. (A 10-μL cell in a 5-mm rotor permits HR even when nearly empty, irrespective of susceptibilities.) The other reason is to make it possible to achieve more uniform packing of solid resin beads of different sizes. If the beads and the liquid solvent in CC have differing susceptibilities, as is normally the case, perfect averaging will occur only if the beads neatly form a full single (or double, etc.) layer on the inside surface of the cell. Otherwise, 15–100 Hz residual linewidth can be expected, even under fast stable MAS. In cases like this, it is beneficial to select cell and bead sizes that allow for more uniform packing. With squishy materials, one can usually spin fast enough to achieve good cylindrical symmetry, but even this is inadequate when there is a large susceptibility anisotropy. For true HR on a single CC bead, it must be held on center and spun about its axis.

The first HR MAS probes employed a modification of the Gay design (*3*, *7*). Stable, slow MAS is possible with this spinner design, in which the bearing and drive surfaces are both on a plastic drive turbine that presses over one end of a thick-walled glass tube. The attractive feature of this design is that with no hardware near the coil, it is very easy to achieve HR by simply using a compensated rf coil, and it is much easier to minimize unwanted backgrounds and work with vacuum-sealed samples. However, its practical spinning rate limit, though about 5 kHz with uniform solids, is often only about 2 kHz with liquid samples, as the bearing lacks the stiffness often needed to control vortex resonances. Other limitations of early HR MAS probes included low-power decoupling, limited VT range, large thermal gradients, fixed tuning, and fixed angle.

Under ideal conditions, the spinning speed needs to be 15 times the full-width half-height (FWHH) of a Lorentzian line for the amplitude of the first spinning sidebands to be 0.1% of the parent lines, and the static water linewidth in tissues is often ~ 0.7 ppm with nearly Lorentzian shape. Hence, over 3 kHz is required with typical tissue samples for protons at 300 MHz. (Obviously, much higher speeds are needed for the rigid components.) At least 5 kHz is typically required at 500 MHz when spinning sidebands need to be below 0.1%. However, excellent resolution and sidebands below 0.3% are often obtained at 1.5 kHz, where heating is negligible and instabilities with low-viscosity liquids are not likely.

Angle setting accuracy is usually not critical in HR MAS. How close the spinning axis needs to be to 54.736° depends on the relative narrowing that is to be achieved. Narrowing by a factor of 40 (the typical case) requires angle setting accuracy of $\pm 2^0$. However, the accuracy requirement is nearly quadratic with narrowing in the extreme narrowing case (*1*), so narrowing by a factor of 1000 (which may be possible for some solvents with poor susceptibility match to the cell) requires angle accuracy of a few minutes.

Fast HR MAS and Centrifugation

With an understanding of what does and does not average under MAS, many of the common solids spinners (*8*, *9*) can now be modified for HR MAS without much difficulty—at least for applications where line shape is not critical. The largest magnetism problems are usually the coil leads, lead

supports, optics, and adhesives. After that, it is the coil itself, exhaust holes (in the Doty supersonic design), VT nozzles (in the former Chemagnetics design), and manifolding. Line shape is largely a matter of having a sealing cell that confines the sample to the homogeneous region with absolutely no leakage (the thin film between the plug and the cell must be no more than several monolayers in thickness), but numerous additional details are also important. However, the design of a versatile commercial product for liquids and biological solids is more complex, especially if HR variable angle spinning (HR VAS) is required, as here one must make the spinner look magnetically more like an ellipsoid and deal with long, flexible leads, as discussed later.

Centrifugation of a dilute solute of molecular weight W, partial specific volume V, and diffusion constant D in a homogeneous solution of density ρ at high centrifugal fields is often characterized by a sedimentation velocity v_s

$$v_s \cong \frac{WD(1 - \rho V)}{RT}\omega_r^2 r_s \qquad [2]$$

where R is the universal gas constant (8.314 J/mol K), T is the absolute temperature, and r_s is the sample cell radius (*10*). Inserting typical values for the $H_2PO_4^-$ ion in water, for example, at 9 kHz ($W = 97$; $D = 8.8\text{E}{-10}\ \text{m}^2/\text{s}$; $\rho V = 0.65$; $r = 1.95$ mm) gives $v_s \sim 0.25$ mm/s (W and D are approximately inversely related, but the product generally increases slowly with W). From the above equation, one might expect the solute would eventually completely settle out with very weak centrifugal fields or gravity alone. This is, of course, not the case because of thermal agitation or Brownian motion, which gives rise to back diffusion and a concentration gradient within each partition. In the case of tissues, the relevant partitions are the tissue cells as long as they are not ruptured and diffusion across the cell walls is negligible. With a cell diameter x of 4 μm, the diffusion time $\tau \sim x^2/\pi D$ is about 6 ms, giving a mean intracellular diffusion velocity $v_\tau \sim x/\tau$ of 0.6 mm/s. Obviously, for sufficiently small cells, v_τ could always be greater than v_s, and there would be little concentration gradient even under fast MAS. The mean diffusion velocity v_τ is inversely proportional to the partition size (as long as it is small compared to the spinner cell radius), while the sedimentation velocity is proportional to $\omega_r^2 r_s$. For CC or liquids MAS, some radial concentration gradients can be expected at rotational rates above 1800 Hz. If the susceptibilities of the solute and solvent are quite different, this may cause a radial BMS gradient and partially explain the broadening that has been reported for CC above 5 kHz, although we have not been able to detect significant line broadening from this effect alone. It also may cause aggregation (and possibly severe broadening) either near the perimeter or central vortex for suspensions or when the solution is near saturation. For example, the cream separates in homogenized milk at about 2.5 kHz in a 3.6-mm cell and concentrates along the central vortex, but the effect on the simple ^{1}H MAS spectra is barely detectable (*11*).

At a spinning rate of 1200 Hz, the centrifugal pressure for water in the 90-μL sample cell described earlier is < 1 atm at the perimeter, but it increases quadratically with frequency (8). The mean operating relative pressure in most joints in animals is around 0.1 MPa (1 atm), and peak pressures may exceed 15 MPa, equivalent to $\sim$ 17 kHz rotation in a 3.9-mm-diameter cell. A more significant parameter governing cell rupture would be tissue shear strength, which often ranges from $\sim$ 0.1 to $\sim$ 10 MPa. However, fluids cannot support shear stresses, so cell rupture is not likely as long as extracellular fluids surround the cells. Spinning of tissues and membranes at several kilohertz causes concentration gradients in the free extracellular components.

Higher spinning speeds are often beneficial. For example, linewidth of the major lipid line in ground beef at $\sim$ 40°C, 300 MHz, was shown to decrease from 20 Hz at 2 kHz MAS to 5 Hz at 18 kHz, although there was considerable cell rupture in these 3.4-mm-inner-diameter (ID) sample cells for MAS above 14 kHz (*11*). Of course, it was necessary to precool the bearing gas to below 0°C, and there may have been $\sim 10^\circ$ error in the actual sample temperature in these experiments.

OTHER PROBE FACTORS IN NMR RESOLUTION AND LINE SHAPE

The discussion thus far and in Part I has focused on the critical susceptibility effects of the coil, coilform, and sample on resolution, although resolution is often limited by other effects—most of which we will ignore in this article, such as residual dipolar or quadrupolar broadening in solids or restricted molecular motion in macromolecules. However, we will briefly discuss a

number of secondary factors affecting resolution that must be considered in HR probe design.

Shims: Capabilities and Limitations

The primary purpose of the B_0 shims (whose name comes from the original technique for homogenizing the field in an electromagnet) is to correct inhomogeneities from the magnet, probe structure, and major components within the probe. To simplify the manual shimming process, the shims must be orthogonal—that is, the integral of the product of the corrections for any pair of coils over the sample volume should be zero. Until recently, each axial gradient was generated from separate, series-connected combinations of properly spaced short solenoidal windings, and each transverse gradient was produced from a set of properly positioned rectangular saddle or "Golay" coils, such that the spherical harmonic functions were approximated (*12*). Some recent designs depart from this tradition by using computer-control of the current ratios in a smaller number of more efficient coils, none of which is associated with a single shim control. With proper mixing, it is possible to obtain more accurate and more efficient production of the desired spherical harmonic, and higher-order functions are more easily obtained (*13*). Obviously, these "matrix" shim coils cannot be driven by conventional shim supplies. Even with the latest coils, the orthogonality condition can be accurately achieved for only one sample size, which is normally the largest sample the shim set is intended to be used with. Hence, there is usually considerable interaction of the adjustments for typical sample sizes. Since an excellent tutorial has recently been published on shimming (*4*) and several articles have appeared on shim coil design in recent years (*14*, *15*), only a few additional comments will be made here.

A massive aluminum structure beneath the tuning elements in an HR liquids probe may produce 0.1 ppm inhomogeneity over a moderate sample region in a perfect probe, but the perturbation is a low-order function because the magnetic source is well removed from the sample. With just the Z-shim (and perhaps a little Z^3), it is easily canceled to a fraction of a ppb. Likewise, two stainless-steel dewared transfer lines on opposite sides of the sample region will give rise to large $Z(X^2 - Y^2)$ gradients (along with large Z, Z^2, and Z^3 terms), but again, the field would be easily correctable as long as they stop at least $0.7r_g$ from the sample, where r_g is the radius of the shim coils, and as long as the perturbations are within the corrective ranges of the shims. The closer the magnetic sources get to the sample, the greater will be the short-range gradients and the less effective the shims become in correcting their perturbations.

When the sample is completely confined to a region where the B_0 inhomogeneity is much less than the natural NMR linewidth of a collection of spins under rapid isotropic motion with a transverse relaxation time T_2, the free induction decay (FID) decays according to $\exp(-t/T_2)$ and the Fourier transform (FT) line shape is given by the Lorentzian function:

$$L(f) = \frac{AT_2}{1 + 4\pi^2 T_2^2 (f - f_0)^2} \qquad [3]$$

where A is the peak amplitude of the FID. At full width $2(f - f_0) = 1/\pi T_2$, the relative amplitude, L/AT_2, is 0.5. The width at 10% of maximum height is 3.00 times FWHH. The width at 2% is 7.0 FWHH; at 0.55%, it is 14.1 FWHH; at 0.11%, the width is 30.2 times the FWHH. The widths at 0.55% and 0.11% of maximum (the relative height of the satellites in $CHCl_3$) are commonly used in specifying line shape.

Even under the best of conditions, 1 ppb homogeneity can be achieved only on a 5-mm sample over a length of about 18 mm; but, as previously noted, the sample must extend about 15 mm above and below the active region in a liquids probe unless precisely matched susceptibility plugs are being used. This means that normally, there will be sample in regions of inferior homogeneity, from which there will be some signal since the rf cannot be completely limited to the central region. This poorly resolved signal appears as excess contribution to the baseline width and is particularly large when the coil leads are unshielded. However, line-shape problems (*16*) in modern HR liquids probes are more likely due to near-field perturbations (chip capacitors on the coil, adhesives, coil crossover insulators, etc.) than to signal pickup from unshielded leads, as HR probe vendors have paid careful attention to lead shielding for the past 15 years. Spatially selective pulse sequences (*17*) are less effective in addressing near-field problems than lead shielding problems. In HR MAS, the samples must be completely confined to the central region, and susceptibility matching of the cell is not important. Line-shape problems would then come from near-field perturbations.

Even though the shim power supply normally increases linearly with shim coil diameter, the corrective range of the shims still decreases roughly as $r^{n-0.5}$, where n is the shim order and r is the ratio of shim coil diameter to sample diameter. Thus, a Z^6-shim in a wide-bore (WB) magnet (73-mm shim bore) is likely to have $< 5\%$ of the corrective range of the Z^6-shim for the same size sample in a narrow-bore (NB) magnet (40-mm shim bore). Table 1 shows typical maximum corrections as a function of z as measured along the axis in a shim set from the late-1980s in a 300-MHz WB magnet. The large range of the Z^2-shim is needed for such perturbation as short samples, heavy Pyrex dewars around the sample region, and thick support disks above and below the coilform. (The Z-shim in this case was underpowered for some cryogenic probes and for short, asymmetric samples.) Note that large corrections with high-order shims are possible only near the edges of large samples and the functional dependence is not very close to ideal above second order. Modern shim sets generally have greater range and more accurate functional response or "spectral purity."

Shimming the HR MAS probe is quite different from the conventional liquids probe because the plane averaged by the spinning is rotated approximately 55° and because the spin rate is fast enough to fully average any odd-order inhomogeneities in the plane transverse to the spinning axis. Thus, if the spinning axis lies in the YZ-plane, the X- and X^3-shims have no effect, and the Y-shims are most significant. However, since only the field gradient component along the spinning axis has much effect, the Y- and Z-shims have similar effects—just different magnitudes. Also, since the sample volume is normally quite small, there is no reason to use any shim over third order. A good procedure is as follows: First, do a rough shim while spinning at ~ 2 kHz using only the Y-shim (assuming alignment in the YZ-plane). Then stop spinning and do a rough non-spinning shim using X and Z, but avoid large adjustments if they are not particularly beneficial, as it probably indicates a bubble is present and adjustments could be counterproductive. Then spin up to 2 kHz and adjust Y and Y^3. A little further improvement will be possible by touching up YZ, $X^2 - Y^2$, XY, Z^3, and fine Z if the Y control is not fine enough. Working with the other shims is not likely to be productive in a well-designed probe—the Z^2-shim is particularly ineffective under MAS because it is actually (approximately) $2Z^2 - (X^2 + Y^2)$. If the spinning axis is not precisely in the YZ-plane, the X-shim will have an axial component and its effect will be similar to the Z-shim, but the above procedure will still work well. If it is more convenient to align the spinner in the XZ-plane, simply interchange X and Y in the above procedure. Shimming for static resolution is quite different and requires additional work with all of the shims through third order. Some improvement in static shimming is theoretically possible by adjusting groups of shims in concert in specific ratios (*14*), but in practice, this does not appear to be beneficial.

Table 1 Maximum Corrections (ppm) of Axial WB Shims

z-Location (mm)	Shim Range (ppm)				
	Z^1	Z^2	Z^3	Z^4	Z^5
0	0.0	−0.60	0.08	−0.08	0.05
5	0.29	0.12	0.25	0.08	0.13
10	0.60	1.6	0.45	0.2	0.07
15	1.00	5.5	1.3	0.7	0.02
20	1.45	10.0	3.3	2.5	0.25

The effective averaging of large, transverse linear gradients in HR MAS may be used to suppress backgrounds from tuning capacitors or other probe components. Applying a high Z gradient can move the interfering background from a capacitor out of the spectrum, and the sample can be reshimmed to essentially the same resolution with the Y (or X) shim.

Thermal Gradients

The effect of density changes, whether by temperature change or pressure change, has been studied for many samples from the early days of NMR. The effect of the radial pressure gradient in MAS on line broadening is usually negligible, as shifts typically range from 1 to 15 ppb/MPa for the common nuclides [although they are occasionally an order of magnitude larger for very large ions (*18*) and the maximum centrifugal pressure is usually about 4 MPa (typical 4-mm sample at 7 kHz), although it may go over 60 MPa for high-density samples at maximum speeds. However, thermal shifts are often an order of magnitude greater. Lead nitrate has been shown to be particularly useful as a thermometer because of its large shift coefficient (sufficient to obscure most other sample and probe effects) and exceptional linearity. The chemical shift of ^{207}Pb

in $Pb(NO_3)_2$ has a slope of ~ 0.75 ppm/°C with a standard deviation of 0.002 ppm/°C between -110°C and $+130$°C (*19*). However, the pressure dependence of the chemical shift of $Pb(NO_3)_2$ is also large, roughly -100 ppb/MPa (*18*), and must be considered for temperature calibrations above ~ 5 kHz in a 5-mm rotor. Fortunately, the slopes are several orders of magnitude smaller for most proton and carbon NMR, but even at 0.003 ppm/°C (a more common value), it is obvious that temperature differences (we will often use the technically incorrect jargon "thermal gradients" for "temperature differences within the sample") may need to be a fraction of a degree for HR in some cases. This is straightforward only under conditions of low decoupling power in small, conventional, liquids probes near room temperature.

In conventional liquids probes with moderately high VT control gas flow (25 L/min), the gradients on the surface of an outer HR decoupling coil on a quartz form can be kept below 50°C at 10 W average power, while the thermal gradients induced in a spinning low-loss sample will be in the range of 0.2–2°C (*20*). However, the gradients in lossy samples can be an order of magnitude greater unless proper measures are taken in the coil design to minimize electric fields within the sample, as most of the power can go directly into one end of the sample. The situation may be improved by using a silicon nitride or alumina coilform, as their thermal conductivity is more than an order of magnitude greater than that of quartz, Pyrex, or macor. The more common solution at high fields is to use multiple-pulse or adiabatic decoupling techniques that permit efficient broadband decoupling with much lower power and use low-inductance decoupling coils to minimize dielectric heating.

For solids, high-power decoupling is usually beneficial, though normally at $< 10\%$ duty cycle. Also, only 20–60% of this power is dissipated in the decoupling coil and coilform (the balance goes into capacitors, traps, sample, leads, etc.). The order-of-magnitude reduction in thermal gradients from silicon-nitride (or alumina) stators and ultra-low-inductance decoupling coils with quadrupolar electric fields (*20*) is particularly beneficial with biological samples. For example, we measured an apparent thermal gradient of just 0.7°C in a 70-μL sample with 12 W average decoupling power (120 W, 10% duty cycle) in a 5-mm spinner at 4 kHz and 40°C that was linear with average power (*11*).

The farther the desired sample temperature is from room temperature, the greater will be the additional gradient induced from imperfect thermal insulation or air-flow design. This contribution to the thermal gradient may be as small as 1.5°C at 300°C in well-designed extended VT probes for small samples (0.1 mL) with either conventional HR liquids or solids, and twice that for large samples (1 mL). For example, we measured < 3°C thermal gradient at 350°C in a 10-mm HR liquids probe designed for use to 500°C. However, gradients > 40°C at 250°C or at -180°C have been reported in some commercial solids probe designs for small samples where the bearing and drive gases are at room temperature and a third gas stream is used to control temperature at the central region of the rotor. The key factors for low thermal gradients are high-conductivity ceramic coilforms, VT control of all gases near the sample, and adequate thermal insulation outside the coil region.

Finally, fast MAS is another major contributor to thermal gradients in the sample even though it completely averages azimuthal thermal gradients. In most commercial MAS designs, the axial thermal gradient is dominated by a linear component, as most of the drive torque is supplied at only one end and a Bernoulli axial bearing (possibly providing a portion of the drive torque) is located at the other end. With an efficient drive turbine, there is considerable temperature drop (typically 10–30°C) in the drive gas as work is extracted. This work reappears as heat in the radial bearings and, to a lesser extent, in the rf coil or coilform and Bernoulli bearing. Frictional power is typically 5–10 W at each end at top speeds for a 5-mm rotor. Temperature rise in the radial bearings, where mass flow is much lower than in the drive turbine, may exceed 140°C at top speeds with a zirconia or macor stator and zirconia rotor (which is sufficient to cause a macor stator to shatter from thermal stress alone). If flow rates, axial bearings, radial bearings, drive efficiency, and drive power are not identical at both ends of the spinner, the linear thermal gradients may be large, especially if the radial bearings are not thermally coupled by a high-thermal-conductivity coilform.

Most MAS probe manufacturers have avoided the use of an internal coilform. The absence of the uniformly spaced surface adjacent the rotor surface exacerbates thermal gradient problems by yet another mechanism. The large variation in frictional heating beyond the axial ends of the rf

coil (where the rotor surface is not near the wire or bearings) compared to the center (where any point on the rotor surface is close to the wire for over half the rotor period) gives rise to a quadratic thermal gradient. With a freestanding or internal rf coil and a zirconia rotor in nonsymmetric spinner designs, thermal gradients > 60°C have been reported at highest speeds.

In recent symmetric designs with an internal coilform, the radial clearance in the gas bearings at either end is about 0.026 mm, while it is about 0.2 mm in the central coilform region to permit inward axial flow and exhaust of the bearing gas, as this improves bearing stiffness (*22*). Thus, frictional heating per length in these fast spinners is much less at the center (~ 0.2 W/mm) than at the ends. The most important parameter in minimizing quadratic thermal gradients is maximizing the ratio of axial thermal conduction to mean frictional heating in the coilform region. However, a thick coilform well spaced from the rotor decreases the filling factor, so effective heat exchange around the coil region is also required. To improve the heat transfer coefficient, a shell or housing is desired to constrain a turbulent, high-velocity circumferential flow in this region. Obviously, the bearing gas must be introduced at a temperature well below the desired sample temperature (by up to 90°C) during fast MAS, but thermal gradients are still below 2°C. Temperature calibration as a function of spinning rate is not difficult, as the heating effects are quite reproducible. This is not the case with decoupling heating, which makes it important to minimize electric field heating of the sample and rotor.

Figure 2 shows FWHH linewidth of 45 Hz on a 70-μL sample of lead nitrate at 13 kHz MAS, 60°C in a prototype HR MAS spinner (without the VT shell) at 62.7 MHz (7 T). The maximum centrifugal sample pressure was calculated to be ~ 40 MPa, giving an expected pressure baseline broadening of ~ 4 ppm, although only ~ 3 ppm was measured. (A 19-Hz FWHH linewidth was measured at 4 kHz, and the natural linewidth at 13 kHz was estimated to be ~ 2 Hz.) The effects of linear thermal gradients on resolution may be shimmed out using the room temperature (RT) transverse shims just as effectively as small B_0 gradients may be, although the corrections are dependent on spinning speed, decoupling power, and temperature. However, higher-order shims are ineffective on small samples, and radial gradients cannot be affected by shims. Thus, it appears that the actual spinning-induced thermal gradient was a small fraction of a degree at 13 kHz and most of the broadening was from the pressure gradient.

Of course, much HR MAS may be performed at 20% of the maximum rotational rate, where spinning-induced thermal gradients are lower by

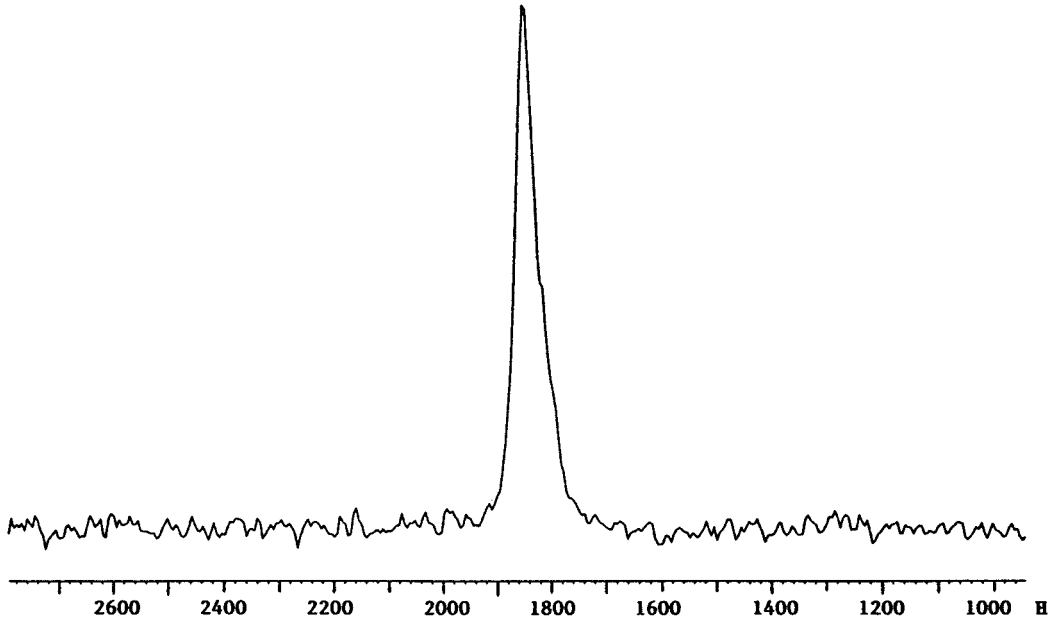

Figure 2 Pressure and thermal gradient broadening in $Pb(NO_3)_2$ HR MAS at 13 kHz, 60°C.

a factor of 25–50 and generally acceptable even with axially asymmetric spinner designs. Frictional heating for laminar flow conditions at moderate speeds is quadratic with surface speed, but it increases more rapidly as the surface speed approaches the speed of sound. Also, it can jump abruptly by more than a factor of two in high-speed bearings in a transition from laminar to superlaminar flow during the formation of Taylor vortices (*8*). However, rf-induced thermal gradients (especially for unbalanced circuits) are often larger than spinning-induced thermal gradients. VT-induced gradients are usually the smallest—except when some of the control gases are not temperature regulated, in which case VT-induced gradients usually dominate at extreme temperatures.

With such an enormous reduction in thermal gradients from having a silicon-nitride or alumina coilform (even when compared to having a silicon-nitride *rotor* and zirconia *coilform*), one might ask why it is often not used. There are a number of factors in the answer. The coilform decreases the filling factor by several percent and makes it more difficult to prevent rf noise (from minor breakdowns) during high-power decoupling (it requires rf balancing and low-inductance coils at high frequencies). Alumina is less desirable for the coilform because of its lower impact resistance, incompatibility with standard methods for precision drilling (Nd:YAG laser), and enormous ^{27}Al background signal. Silicon nitride is much more difficult to grind than zirconia or alumina, and convenient shapes of high-purity grades are not stocked by any supplier. Thus, precision silicon-nitride parts in small quantities are quite expensive. Another issue is that the low thermal expansion of silicon nitride makes it incompatible with zirconia rotors in extended VT operation (either at high or low temperatures), and high-quality silicon-nitride rotors have only recently become available at reasonable cost.

The very long T_1 of ^{29}Si in high-purity Si_3N_4 ($\sim$ 30 min at high field) often allows it to be used even for silicon NMR. Of course, where silicon and aluminum backgrounds are critical, a symmetric zirconia spinner with an internal coilform permits reasonably low thermal gradients, but more difficulties in shimming out their effects can be expected. Unfortunately, available symmetric drive designs are not compatible with sample eject, but a reconfigurable design is discussed later that partially addresses this issue.

Sample Homogeneity

For solutes in uniform liquid solution, there is no concern about sample homogeneity as long as gas evolution, precipitation, aggregation, vortexing, or convection do not occur. With solids, nonuniformity is more likely to be a source of broadening.

Uniformity on a macroscopic scale is required for accurate MAS averaging of BMS effects throughout the sample cell, as previously mentioned with regard to the packing of beads into cells. Samples packed uniformly enough for stable spinning are not necessarily packed well enough for adequate resolution—especially with long, thick-walled rotors, which tend to tolerate greater sample imbalance.

The effective sample density of a powder is often 5–12% less than theoretical density even when it appears to be tightly packed. Thus, there is still a substantial fraction of the particles in the highly nonuniform fields near an air–solid interface. While theoretical analysis indicates that inhomogeneity from particles of a material having isotropic susceptibility should fully average for any particle shape and orientation under MAS (*23*) as long as the sample is macroscopically cylndrically symmetric, our experiments suggest that even with such materials, there are minor residual susceptibility broadening effects in powders. We find the MAS of powdered solids with large internal mobility (such as silicone or adamantane) typically gives lines about 0.01 ppm broader than the MAS of a solid plug of the material at speeds four times the static linewidth.

B_0 Stability

High-resolution probes for liquids nearly always include ^{2}H lock. It is essential in any extended HR run since the magnet drift in a fraction of an hour (or an external fluctuation) may be comparable to the linewidth and thus degrade resolution and sensitivity. Conventional solids probes have not included a lock channel, as the extended runs were usually on samples with broad lines. However, the HR MAS probe often requires lock.

Even when resolution is not high, cryogenic extended VT MAS solids probes will benefit from a lock channel, as they often contain large dewars and structural components of relatively magnetic alloys. Although the inhomogeneity from these components can usually be adequately shimmed, there is often a large temperature-dependent B_0 shift in these probes that is difficult to calibrate,

as the temperature of the offending material depends on recent heating and cooling history and room-air flow as well as on current sample temperature. The improved dewar alloys currently under development should improve unlocked B_0 stability of some XVT probes by an order of magnitude in the near future (*24*).

B_1 Homogeneity

High rf homogeneity may not be critical in many single-pulse experiments, but it is crucial to obtaining HR in multipulse techniques (*25*). Also, it has recently been shown that sensitivity during fast cross polarization (CP) MAS requires high rf homogeneity at both frequencies, since the Hartmann–Hahn match is offset by the spinning frequency (*2*, *26*). While conventional saddle coils had poor B_1 homogeneity and efficiency compared to solenoids (*27*), this is not the case for the numerically optimized slotted resonator (SR) (*28*).

Table 2 summarizes effective inductance, relative rms B_1 inhomogeneity σ, filling factor η_F, tank Q_0, and loaded Q_L at 500 MHz for several widely used high-frequency NMR coils. For η_F and σ measurements and calculations, the sample region was assumed to be a cylinder 4.2 mm in diameter by 8 mm long (110 μL), which is short for conventional solids and HR liquids but long for HR MAS, and the internal coilform outside diameter is 6.2 mm. Inductance, η_F, Q_0, and Q_L are measured values with minimum leads and ATC-100B 1000-V chip capacitors. The sample for Q_L was a 90-μL, 0.3-mol saline sample (resistivity ~ 0.3 Ωm, or conductivity ~ 3.3 S/m). [Filling factor, Q_L, and σ are discussed in more detail elsewhere. We define magnetic filling factor in the conventional manner for circular polarization, but half that for linear polarization, not one fourth, as mistakenly indicated previously (*29*).] The coil lengths are such that the mean transverse B_1 in the end planes of the sample is approximate 85% of that near the center. For these coils at ≤ 200 MHz, increasing the number of turns also improves homogeneity, unloaded Q_0, and filling factor; but Q_L is degraded with lossy samples and the increased voltages reduce the maximum decoupling field that can be obtained. The length and diameter choices represent a moderate emphasis on B_1 homogeneity within severe length constraints, as for a fast MAS spinner in an NB magnet. In most cases, further increases in length could reduce σ by at least 30% and improve Q_0, but η_F would be degraded for a fixed sample length. The η_F and σ values shown for the solenoids are for the low frequency limit; their actual η_F at 500 MHz is $\sim 70\%$ of that indicated, as self-resonance occurs at ~ 650 MHz on a silicon-nitride coilform.

Coil 1 is the conventional "Hoult solenoid"—a constant-pitch helix of round wire where the gap (spacing) between turns is half the wire diameter (*27*). Coil 2 uses flattened wire, constant pitch, with gaps 25% of wire width (*29*). Coil 3 is a variable-pitch solenoid that uses round wire flattened only over the central turns to a width twice the initial wire diameter and wound with constant gap of 25% of the central flat width (*29*). Coil 4 is the conventional two-turn Ginsberg saddle coil, also often (loosely) called a Helmholtz coil, with window subtended angle of 120°, window inside length of 9 mm, and 1-mm wire diameter (*27*, *30*). Coil 5 is the Kost slotted resonator (*28*), similar to Fig. 2 of Fuks et al. (*16*), or Fig. 8 of Part 1 (*24*), but unsegmented, with 8.4-mm window length and 90° subtended angle in the windows. Coil 6 is a proprietary modification of the Alderman–Grant resonator we denote here as the XC5 coil—similar to the DHT coil described subsequently.

The data in Table 2 are for balanced coils with external shields far from the coil. The presence of a nearby coil (internal or external) or external rf shield degrades all parameters. For example, the

Table 2 Loaded Small Coils at 500 MHz

Coil No.	No. Turns	O.A. Igh (mm)	Type	L (nH)	Q_0	Q_L	η_F (%)	$\mathbf{B}_1$ σ (%)
1	4	10	Hoult solenoid	64	280	85	13*	5*
2	4	10	Flattened solenoid	58	290	82	15*	4*
3	4	9	Doty solenoid	60	300	80	14*	3*
4	2	11	Ginsberg saddle	35	300	240	7	7
5	1	16	Kost SR	11	210	155	9.5	5
6	0.5	17	Doty XC5	5	240	210	9	4

* Below ~ 150 MHz.

degradation is typically more than a factor of three in $\eta_F Q_L$ for an external rf shield diameter 1.4 times the coil diameter, while σ is degraded by anywhere from 10% to a factor of three, depending on the coil design. The XC5 coil maintains considerably better B_1 homogeneity than the Kost SR under these conditions, or when a solenoid is wrapped over it (separated by about 0.3 mm of Teflon or polyimide insulation), which is one of the reasons it is preferred over the Kost coil in MAS, although its primary advantage is its capacitor symmetry which allows it to achieve high B_0 homogeneity and handle much higher power, as will be seen shortly. Also, its self-resonance on the nitride coilform is over 1.6 GHz.

The Ginsberg saddle appears to have higher Q_0 than the Kost coil, only because capacitor Q's are higher at smaller values. (The actual Q of the Kost coil itself is greater than that of the Ginsberg coil.) The problem becomes even more significant in the XC5, where it is necessary to select high-Q capacitors from the lot. The Q's indicated are typical for rejection of the lower quarter of the lot. Special termination and more careful selection have given Q's $\sim 25\%$ higher. The Ginsberg saddle shows low sample loading primarily because of its low filling factor. Sample rf heating is largely determined by $(Q_0 - Q_L)/Q_L$.

A CASE STUDY IN MAGNETISM DESIGN: THE XC5

Our recent investigations of novel NMR probe designs were stimulated by an increasing number of requests for experimental capabilities that were impossible to accommodate with prior technologies: an order of magnitude improvement in resolution and line shape for MAS of semisolids; 120 kHz (or higher) decoupling fields at 500 MHz with large biological samples; order-of-magnitude reduction in thermal gradients in samples under fast MAS and high-power decoupling; simultaneous high-power decoupling of ^{1}H and ^{19}F at the highest fields in a quad-resonance probe; magic angle gradients; greatly improved reliability; goniometer control for oriented samples, etc.

For the past 15 years, industrial competition has forced manufacturers to push available designs to the limits in rf power, operating temperature range, and spinning speeds. Not surprisingly, solids NMR probes of all types have been more prone to failure than liquids probes. A radical change in sample coil topology is required for a significant increase in rf reliability and acquisition times, and the approach we have taken is essentially a constrained numerical optimization of the segmented (half-turn) Kost coil for proton decoupling that permits higher coupling strength with nearly an order of magnitude reduction in ^{1}H rf voltages and electric fields compared to solenoids —without interfering with the other requirements of HR MAS. An *outer* solenoid is used for the multinuclear coil.

Fifth-Generation Cross-Coils

Since the earliest experiments in cross-polarization of solids in the mid-1970s, single rf solenoids were double-tuned (using transmission lines) to ensure equal spatial dependence of the two fields and to achieve highest efficiency at the two frequencies (*29*). It was easy to show experimentally that simple wire-wound saddle coils were less efficient than solenoids by about a factor of three (*27*), and no one would have believed there was much room for optimization of such a simple component. However, there are now several compelling reasons for returning to the cross-coil configuration used in the early days of electromagnets: (a) high decoupling in biological solids with minimum sample heating, (b) compatibility with automatic (pneumatic) sample eject and VAS, and (c) greatly improved performance of H-F-X-Y circuits. The first attribute comes from the quadrupolar electric field of the half-turn coil; the second comes from the fact that single-tuned coils permit *much* longer leads; and the third arises from the magnetic orthogonality of the proton cross-coil and the multinuclear solenoid, which now handles fewer channels.

The progress from Ginsberg to Schneider (slotted resonator), to Alderman–Grant, to Kost, and to the XC5 coil is partially illustrated in Table 2. The primary advantages of the new half-turn cross-coils are their ultra-low electric fields, compatibility with symmetric magic-angle capacitor positioning to permit highest B_0 homogeneity, and improved B_1 homogeneity when a second or third coil is also present.

For ultra-low inductance coils (such as the loop-gaps and slotted resonators) to perform well, the chip capacitors must be within a few millimeters of the coil. Unfortunately, even the least magnetic high-Q ceramic chip capacitors we have evaluated (ATC 175B series) have mean susceptibility ~ 10 ppm, which comes primarily from the paramagnetic dielectrics, and the problem may be

exacerbated slightly from the palladium-silver (25%Pd–75%Ag) electrodes that are normally used for improved reliability and processing. (Custom capacitors with copper-plated silver terminations were found to have similar magnetization.) Heavy copper or silver leads may be added to the chips to reduce their magnetization, but accurate compensation is not possible because of the variability in the dielectrics and electrodes, which makes positioning critical.

Magic Angle Capacitors

In the section entitled "Calculating Fields Produced by Magnetic Materials" in Part I, we saw that B_z from a dipole vanishes at the magic angle and a dipole is equivalent to a current loop I of area A. Since higher-order fields fall off more rapidly with distance than the dipole field, any piece of magnetic material at a sufficiently large distance essentially looks like a dipole. For a uniformly magnetized sphere, the external field is a pure dipolar field, and one need not be far from a cube or a short cylinder before its higher-order components are vanishing small. Thus, the external field perturbation from a 1-kV chip capacitor (about $2.5 \times 2.5 \times 3$ mm^3) or a small air hole in a ceramic coilform should be a minimum at the magic angle with respect to its center.

The fields calculated for a cylinder ($\chi =$ 10 ppm) of 2.5 mm diameter and height, aligned with the z-axis, are illustrated graphically in Fig. 3 Note that B_z on the magic angle just 2 mm beyond the surface (at $r \sim 3.3$ mm) is about 4% of B_z the same distance from the cylinder along the y-axis and about 2% of B_z the same distance from the cylinder along the z-axis. Thus, if the chip capacitors can be positioned near the magic angle with respect to the sample, their static field perturbations are greatly reduced. Of course, their angles with respect to various portions of the sample will span a rather wide range for any close location, so a minimum distance is still required. At least a factor of four improvement in resolution is possible by positioning nearby capacitors such that the vector between each chip and the nearest portions of the sample is approximately at the magic angle. The perturbations in the sample at other locations are more effectively averaged by MAS if the chips are distributed so as to approximate cylindrical symmetry. Thus, a circular distribution of four chip capacitors, one at each magic angle ($\pm 55°$ and $\pm 125°$) at the same axial location, provides a further line-shape improvement of about a factor of three under MAS. Obviously, the same applies to any bearing, cooling, or exhaust holes required in the coilform near the sample. Although these perturbation typically have at least an order of magnitude smaller magnetic moment than chip capacitors, the cubic dependence with distance can make exhaust holes more significant than the chip capacitors if they are close to the sample and not at magic angle or magnetically compensated with diamagnetic collars around the holes.

Figure 4 depicts a method of configuring the leads on a balanced half-turn (Alderman–Grant) Kost coil to efficiently use four magic-angle chip

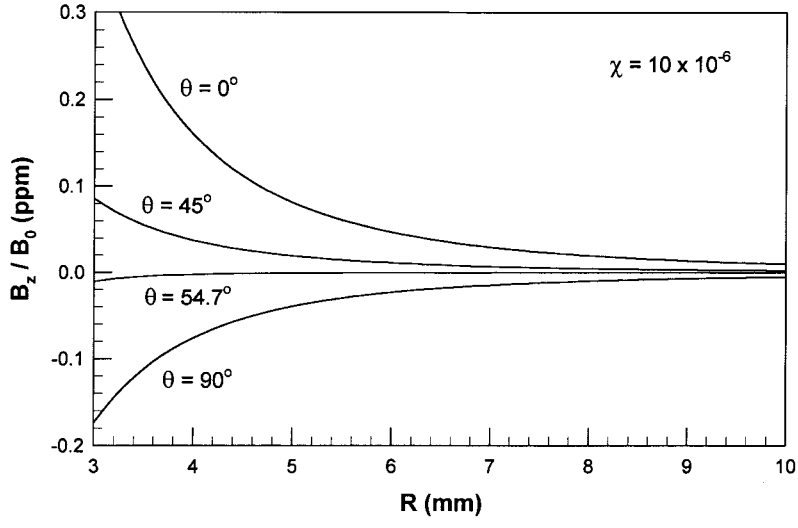

Figure 3 $\delta B_z/B_0$ at several angles near a diamagnetic cylinder, 2.5×2.5 mm diameter.

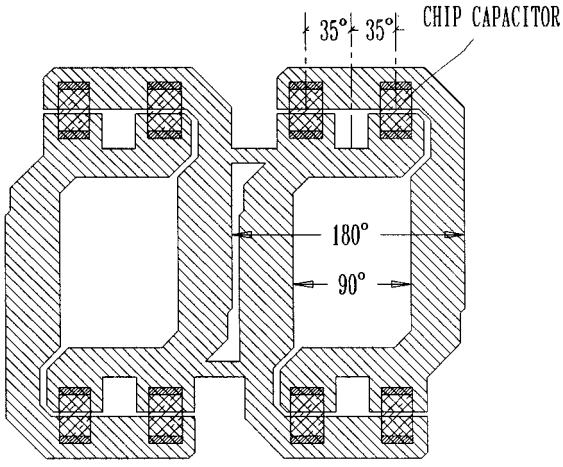

Figure 4 DHT coil with eight magic-angle capacitors, shown laid out flat.

capacitors at each end of the coil (*31*). The foil pattern for this coil, which we denote the Doty half turn (DHT), is shown laid out with eight chip capacitors. Note that the mean angle between the $\mathbf{B}_1$ axis and any chip is the complement of the magic angle, placing the chips at the magic angle when the spinner axis is transverse. When the axis of the coilform is aligned at the magic angle, the angle of the vector between the chips and the nearest portion of the active sample region with respect to $\mathbf{B}_0$ is no longer the magic angle, but line-shape improvement is still about an order of magnitude under MAS compared to an Alderman–Grant coil with four chip capacitors at comparable axial locations. Some additional improvement under MAS is possible by increasing the angles shown in Fig. 4 to 45°, as the normals to the cylinder through the chips is then at a magic angle when the spinner axis is at the magic angle.

The other advantage of paralleling capacitors is improved power handling and Q, as the Q of rf capacitors always decreases with increasing capacitance at a given frequency. This is quite important to FT resolution, as acquisition time in solids (and sometimes with semisolids) may be limited by decoupling heating of the capacitors. Doubling the number of *parallel* capacitors increases the maximum pulse length by about a factor of three, and another factor of two in pulse length is possible if one end of each chip is soldered to a good heat sink (which is now possible owing to the low electric fields), as the thermal time constants of chip capacitors are comparable to long decoupling periods. A large *effective* thermal mass of the decoupling coil is also important with high-power pulsed decoupling to mitigate detuning from pulse heating. That is, either the decoupling coil must be rather massive or it must be in intimate thermal contact with a highly conductive coilform. While these measures go a long way toward improving tuning stability during long pulses (which is critical in many multiple-pulse, inverse, and 2D experiments), it is still beneficial to select temperature-stable (NPO-type) capacitors, which have only recently become available in high-Q 1000-V chips (ATC 700 series). Copper-plated–silver terminations, finished with a gold flash, are available on custom order at a premium price and have somewhat higher Q if carefully soldered on just a small portion of the termination, with care to avoid solder over most of the termination.

While long decoupling periods are essential for HR in FT, very recent advances in spectral data processing using information theory matrix pencil methods suggest that long acquisition times may not be necessary (or even desirable) at some point in the future, as ideal resolution can be obtained from severely truncated FIDs (except perhaps for wideline NMR) as long as enough transients are acquired for S/N above ~ 15 (*32*). However, it is still too early to tell how widely applicable these processing methods will be; decoupling period and duty cycle are likely to continue to be important issues in solids probes for quite some time.

The scale of the DHT coil shown is roughly correct for a 10-mm coilform. For the more typical 6.2-mm coilform (for a 5-mm MAS rotor), the chip capacitors get a little crowded and too close to the active region for HR unless they are accurately compensated. Since this is not practical, it is necessary to mount them on short leads that hold them several millimeters radially away from the sample and provide rough magnetic compensation. Obviously, a coil of this type requires an internal coilform for support. However, HF electric fields are now low enough to permit limited use of epoxy with negligible loss in Q or concern with high-voltage breakdown. The leads may be partially incorporated into the etch pattern. Other improvements have also been developed, and we discussed elsewhere, that improve B_1 homogeneity by about 20% (*33*). The tuning circuits and rf analysis, both for the cross-coil and for the solenoid, will be addressed in more detail elsewhere.

VAS Coilform and Structure Geometry

As indicated earlier, it is rather easy to achieve HR MAS as long as slow-spin HR or VAS is not required. One simply designs the spinner assembly from an ensemble of coaxial cylindrical section (their length is immaterial) and uses a magnetically compensated rf coil. However, for slow-spin HR MAS or VAS, the cylindrical sections must be very long, with their ends far from the sample region, or compensation is required. Our attempts at magnetic compensation of silicon nitride by erbia doping proved unreliable—it was too difficult to ensure uniform mixing. Moreover, there was an unacceptable temperature (and field) dependence, and dielectric properties were degraded. (It is difficult enough to obtain high-purity hot isostatically pressed (HIP) parts (*34*) with sufficiently low iron, cobalt, and aluminum inclusions from final powder milling and injection molding tooling.) Since very long cylinders are out of the question (especially for narrow bore magnets), some geometric compensation is necessary.

Figures 5 and 6 are perspective views of a preliminary version of a 5-mm HR MAS silicon-nitride spinner assembly denoted the XC5 (for "cross-coil MAS, 5 mm"). Perhaps the most significant difference compared to prior MAS designs (*8*, *22*) is that the coil region may be fully accessible so as to accommodate two or even three rf coils with complex capacitor and lead arrangements. The two-part semicylindrical clamshell covers snap (or glue) into position around the coil region and serve only two functions: to confine the highly turbulent VT air flow around the rf coils, and to provide partial passive shimming. The bearing and drive gases are supplied to the appropriate ceramic manifold rings at each end of the stator by metallic air tubes on opposite sides that are fed by slip pins aligned with the reorientation axis. The large pulley affixed to the drive supply air tube permits accurate reorientation under VAS via a "timing" belt. The nozzle caps come in two styles: HR (slow) MAS and fast MAS (symmetric). The long cylindrical symmetry is not apparent from the outside, but it is only the components within a few millimeters of the sample where this is critical.

A cross section of the HR MAS configuration cut on a plane at the complement of the magic angle with respect to the transverse axis is shown in more detail in Fig. 7. The front, open nozzle cap provides most of the drive torque via the front turbine cap, and the rear nozzle cap maintains axial stability via a Bernoulli bearing at the rear rotor tip. In the fast MAS configuration (not shown), the nozzle caps and turbine caps at each end are replaced with a symmetric design similar to the previous "SuperSonic" design (*22*), except for the addition of bearing vent holes in the turbine caps.

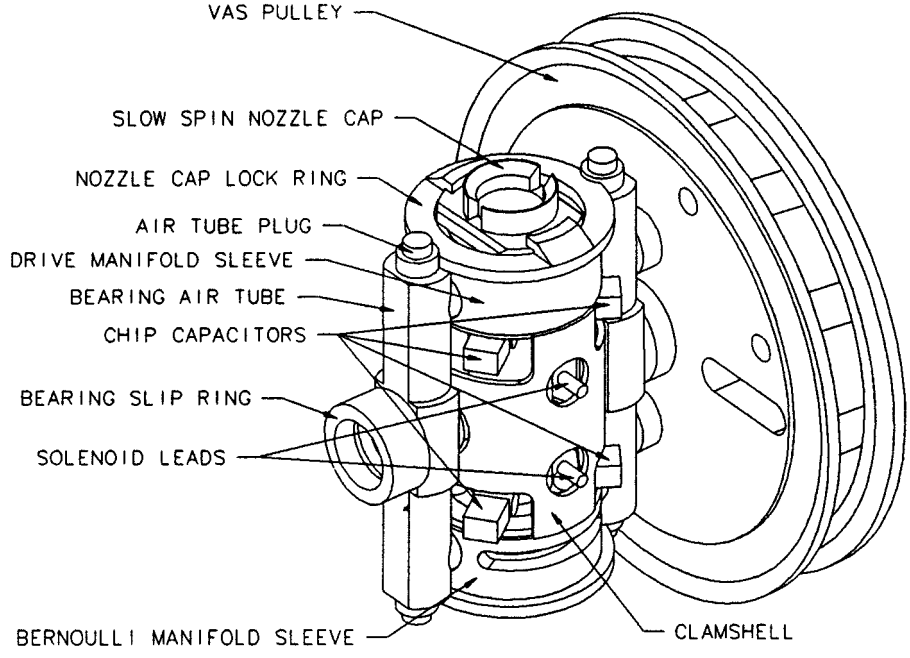

Figure 5 XC5 HR MAS/VAS spinner assembly, with coil cover shells, slow MAS version.

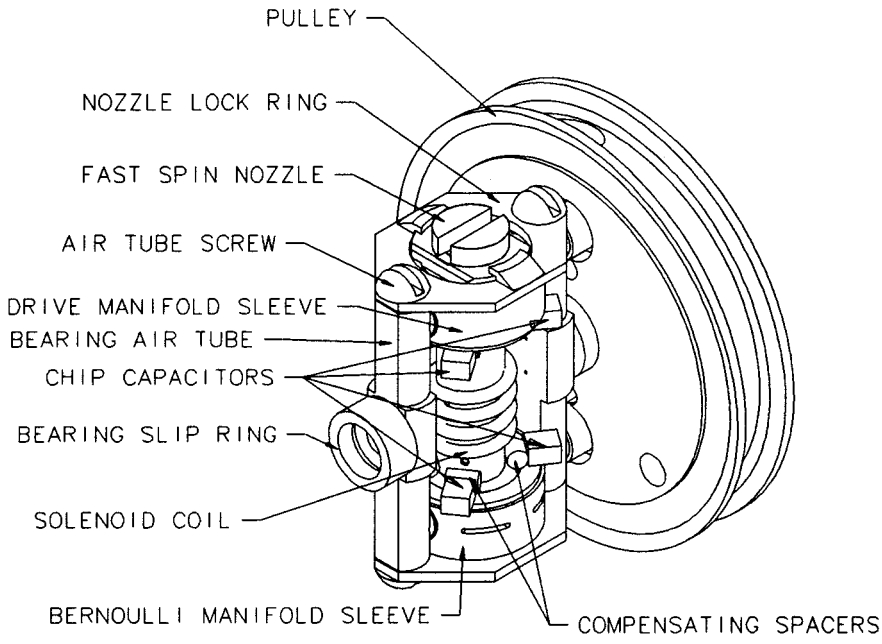

Figure 6 The same assembly with the coil region exposed, fast MAS version.

While the ceramic coilform and stator bearings appear at first glance to have the long, cylindrical symmetry needed for slow HR MAS, static homogeneity depends on a number of subtle details. The exhaust holes required in the coil region for proper operation of the gas bearings are placed as close to the bearings as possible, at the complement of the magic angles, directly under the chip capacitors for the cross-coil. Obviously, the manifold rings required to define the bearing and drive plenums are very short (diamagnetic) cylinders. With the sample confined to the central region, they are far enough away to not present major shimming problems (when the coilform and shell are thick enough), but some improvement in static line shape is possible from magnetic compensation. One method of doing this is to affix a loop of (paramagnetic) tungsten-rhenium thermocouple wire inside the bearing plenums.

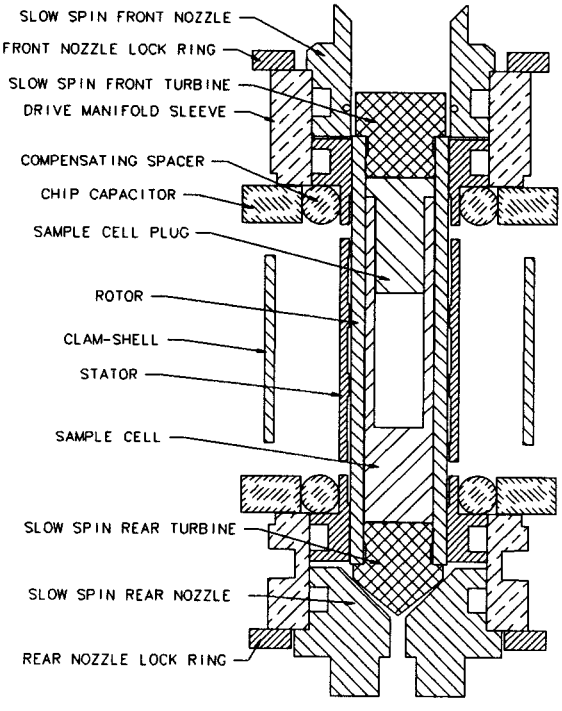

Figure 7 Cross section of the XC5 spinner assembly in the slow MAS (axially asymmetric) configuration.

The cylindrical manifold sleeves are not a problem if the coil-cover clamshells are of the same radial dimensions, as together they approximate a long cylinder. There are numerous holes in the clamshell for clearance of the magic angle capacitors and leads, but their radial location is far enough from the sample for simple compensation with other diamagnetic materials, such as small chunks of silver on the outer ends of the chip capacitors, similar to the compensating spacers under the chip capacitors. The nozzle caps are far enough from the sample region that the perturbations from the differences in their radial dimension and susceptibility compared to those of the coilform and rotor are easily shimmed out except with very long samples. Moreover, the

nozzle caps may be made of metal alloy of susceptibility close to that of the rotor and sample for some improvement. Four of the eight magic angle chip capacitors required by the proton cross-coil are shown mounted on short diamagnetic leads for approximate magnetic compensation. The rf solenoid that is wound over the cross-coil is assumed to have negligible magnetism. It is insulated from the cross-coil by a uniform film of either Teflon or polyimide and normally secured either by heat-shrink Teflon or compensated adhesive—silicone, polyimide, or epoxy.

As shown in Fig. 8, the light pipe (not in the plane shown in Fig. 7) required for optical spin-rate synchronization is probably the most difficult magnetic problem, as it must come in along the reorientation axis rather than the magic angle for compatibility with sample eject and VAS. Here, an all-glass light pipe consisting of clad glass fibers fused together is used, where the cladding glass has lower index of refraction than the core glass to minimize loss in the bend. The mean susceptibility of the light pipe is about -5 ppm. For adequate optical sensitivity, it must come within a millimeter of the rotor, and a small hole (0.6 mm in diameter) is required in the silicon-nitride coilform. Compensation is required, as these perturbations are much too close for shimming to be of any benefit. The optics hole in the stator may be compensated with a small copper or ceramic collar. The metallic air tubes (bearing and drive) on either side would have little effect (as their ends are well removed from the sample region) except for the presence of the holes and bushings in these tubes needed for the light pipe on one side and the VAS pulley on the other side. Thus, a small improvement in shimming can be realized from the use of a zero-susceptibility CuNi alloy for these parts. The VAS pulley is less critical, as the primary transverse gradient it produces is fully averaged under slow spinning and its second-order axial gradient is small because of the fifth-order dependence on distance. RF performance is enhanced by plating any metals near the coil with copper or silver—perhaps with a final gold flash. Replacing structural metallic parts near the rf coil with ceramic increases the filling factor a little, but the effect is too small to justify the cost—except for the manifold rings, as they couple strongly to the solenoid.

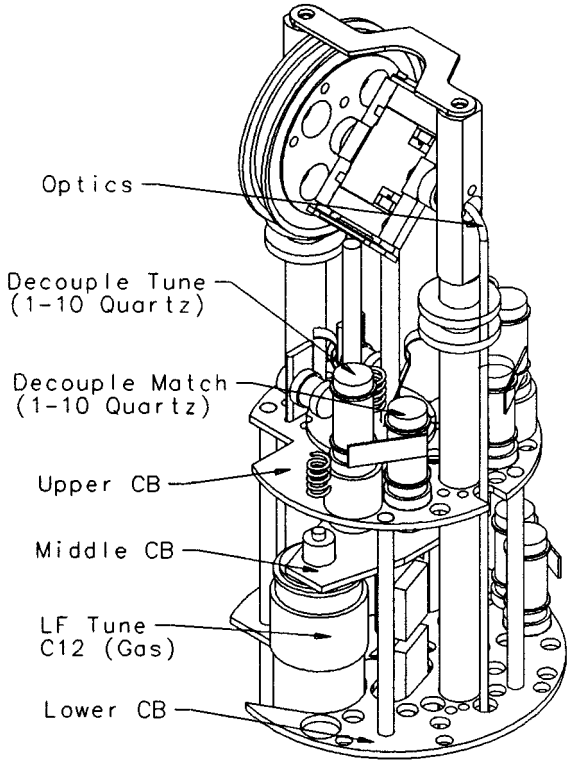

Figure 8 Preliminary version of the XC5 WB probe.

The rest of the structural components shown in Fig. 8 are essentially irrelevant to magnetism design except for temperature-dependent effects on unlocked B_0 stability if standard CuNi, stainless, or NiCrMo alloys are used for the dewars. Even without the extra distance allowed in this structure to accommodate VAS and sample eject, the effects of variable capacitors on homogeneity are negligible as the lowest-order gradients that cause any difficulties (the quadratics) decrease as the fifth power of distance from the offending objects. We have found standard JMC 7584 10-pF quartz variables to have no significant effect on MAS shimming difficulty even when within 5 mm of the outside of the spinner assembly.

The quartz variable capacitors on the upper circuit board for the proton and fluorine tuning would be too far from the coil for efficient multinuclear or double-tuned coils above 300 MHz. However, the voltage standing wave ratio on the leads of fixed, single-tuned coils (as is the case for the proton/fluorine cross-coils) may be reduced by more than an order of magnitude (compared to multinuclear coils) to accommodate long leads with very low loss. The lead losses in the double-tuned multinuclear solenoid are greater, since the double-broadband tuning elements are on the lower circuit board. These losses may be reduced to $\sim 12\%$ using low-impedance flexible transmission lines of a high propagation factor, as de-

Table 3 Factors Affecting Resolution in MAS

No.	Factor Limiting Resolution	Typical Range of Factor	Typical Broadening (ppm)	Maximum Broadening (ppm)
1	Thermal gradients	0.1–60°C	0.1 at 10°C	50 at 60°C
2	Acquisition time	30–800 ms	0.1 at 100 ms	1 at 30 ms, 30 MHz
3	MAS speed (averaging)	6–18 kHz	0.002–0.2 at 10 kHz	2 at 18 kHz
4	Sample inhomogeneity	liquid, CC, chunks	0.01, powder	0.05, chunks
5	Solenoidal Cu rf coil	fine to heavy	0.01 for flat wire	0.03 for round Cu
6	Sample confinement	seated cell, rotor	0.002, cell	0.03, rotor and caps
7	Decoupling B_1	60–120 kHz	0.002–0.02 at 100 kHz	1 at 60 kHz
8	B_1, B_2 homogeneity	4–10% rms	0.001–0.003	0.5, in CRAMPS
9	Coil adhesives	$\chi = 0$ to -9E-6	0.001 for $\chi = 0$	0.02
10	Bearing holes, optics, coil capacitors	$\chi = 0$ to 1E-3	0.001–0.01	0.1
11	Spinning speed: pressure and centrifugation	2–18 kHz	0.001–0.005 at 10 kHz	0.05 at 18 kHz
12	B_0 drift, unlocked	1–10 ppb/h	0.002	0.05
13	Angle-setting errors	0.1–2°	0.002 at 0.4°	0.003–2 at 2°
14	*X*-, *Y*-, *Z*-shims, and other probe components		0.002	0.1 (cryo probes)

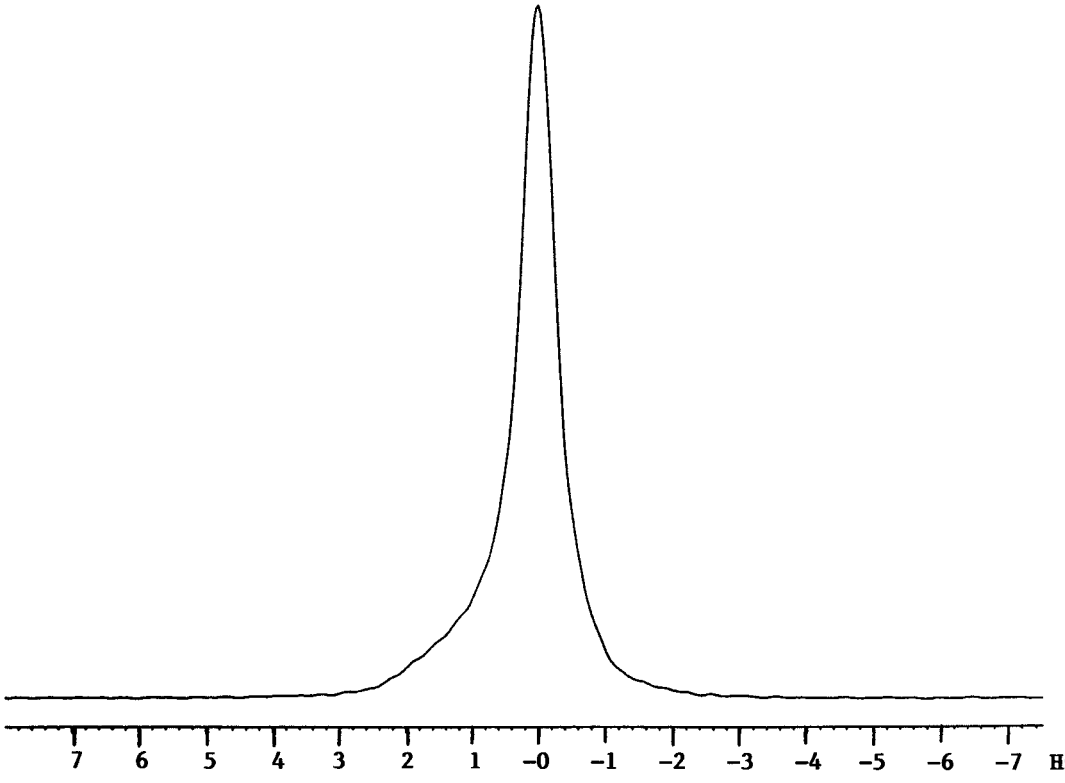

Figure 9 Line shape (10% $CHCl_3$ in acetone-D_6) at 300 MHz for a 60-μL sample in the XC5.

scribed elsewhere. The most significant fundamental losses are the rf eddy current interactions between the orthogonal rf coils, amounting to about 15% loss in $\eta_F Q_L$ for the solenoid and about 40% for the proton coil at 500 MHz, but their significance decreases rapidly with increasing frequency. These and other rf problems are addressed in more detail elsewhere along with other design issues (*31*, *33*).

CONCLUSION

While it may appear that the order-of-magnitude resolution improvement in HR MAS/VAS probes comes at the price of an order-of-magnitude increase in complexity, this is really not the case. It is more dependent on a better understanding of several simple symmetries and better control of materials properties, along with some innovative approaches to ultra-low-inductance coils, circuits, leads, and spinner designs. From our perspective, the probe design factors affecting resolution appear to be toughly in the order indicated in Table 3, although the order depends heavily on the mix of application being run on the probe. Figure 9 demonstrates proton line shape on a 60-μL sample of 10% $CHCl_3$ in an H-X-Y XC5 probe at 300 MHz. For this prototype WB probe, the FWHH was 0.65 Hz, width at 10% was 2 Hz, at 0.55% it was 8 Hz, and at 0.11% it was 14 Hz. Figure 10 shows the ^1H spectra (unlocked, nt = 4) for 70 μL of 0.1 mol sucrose in 99.9% D_2O in the same probe.

The magnetism issues addressed here are only one, albeit important, aspect or the HR MAS probe design problem, and other aspects will be addressed elsewhere. Special materials development work is continuing, especially in the areas of adhesives, ceramic metallization, and custom alloys, to support the never-ending expansion of applications of HR NMR.

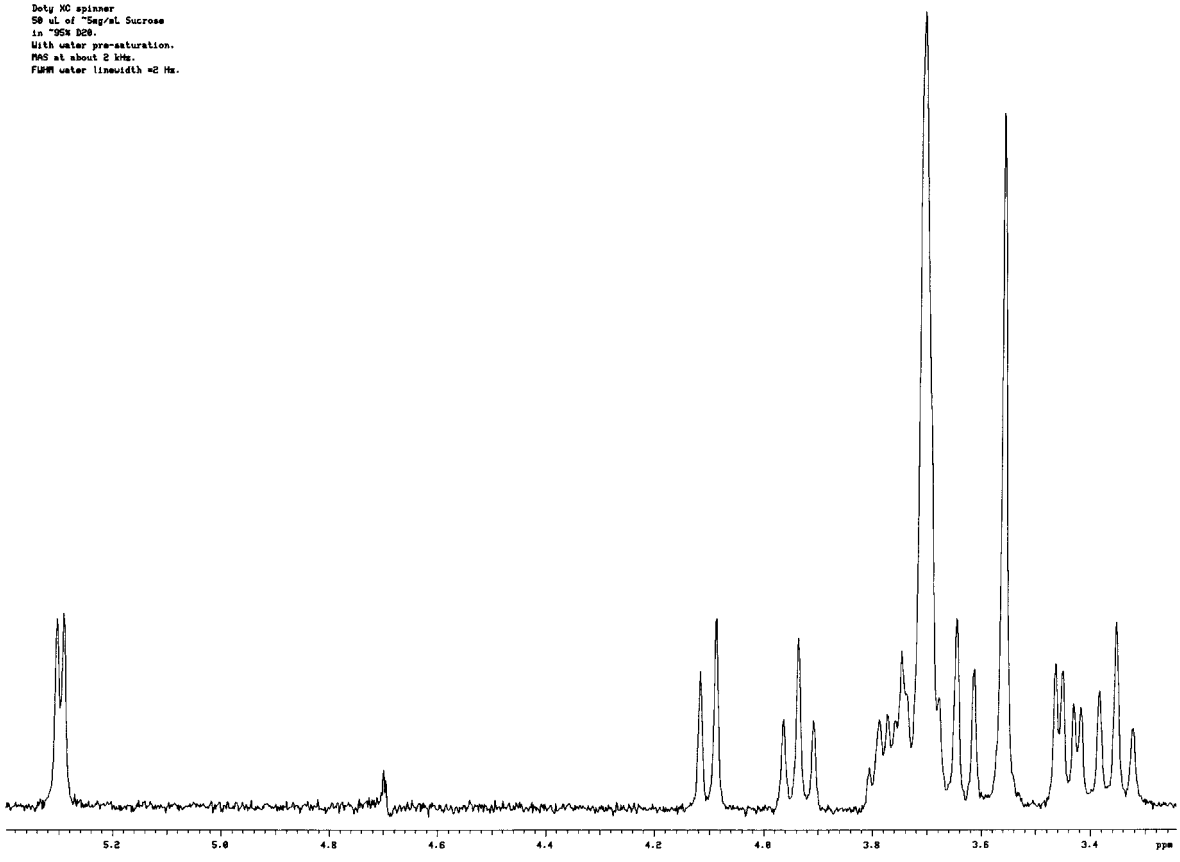

Figure 10 300 MHz ^1H spectra for 70 μL of 0.1 mol sucrose in D_2O at 2 kHz MAS.

PART II: REVIEW QUESTIONS

1. An air bubble in an MAS sample cell with a semiliquid sample will
   a. severely degrade static resolution.
   b. degrade MAS resolution somewhat.
   c. make it more difficult to spin.
   d. make it more likely to leak.
   e. all of the above.
2. For spinning sidebands from the major lipid and water resonances in tissues to be below 0.1% at 500 MHz in ^{1}H MAS, the spin rate generally needs to be at least
   a. 50 Hz b. 150 Hz c. 500 Hz
   d. 1500 Hz e. 5000 Hz
3. Cell rupture and concentration gradients within tissue cells in a 5-mm rotor may be significantly exacerbated by MAS above
   a. 8200 Hz b. 500 Hz c. 1500 Hz
   d. 5000 Hz e. 14,000 Hz
4. HR MAS shimming may have exceptional requirements in which of the following ways:
   a. Needs high fourth-order transverse shim current.
   b. Requires a magic angle gradient shim.
   c. Benefits from extrafine control on the transverse linear gradients.
   d. Benefits more from axial shims above fifth order.
   e. Requires exacting balance between the linear shims to achieve the magic angle gradient.
5. When a liquid sample fails to shim easily under HR MAS in a probe that normally shims well, it probably means
   a. The probe has been inserted at the wrong orientation.
   b. The sample is probably not in the sweet spot.
   c. Some sample has leaked from the central cavity and is trapped elsewhere.
   d. The sample is not closely matched to the susceptibility of the cell.
   e. The cell has too large an air bubble.
6. Large thermal gradients in MAS are most likely caused by
   a. Fast MAS in spinner designs with axially asymmetric drive.
   b. High-power decoupling with unbalanced high-impedance decoupling coils.
   c. Lack of adequate VT control of bearing and drive gas.
   d. The absence of a high-conductivity ceramic coilform.
   e. All of the above.
7. Which of the following statements most correctly compares the segmented Kost coil (or DHT coil) to the four-turn solenoid at comparable size, B_1, and B_0 for high-field decoupling.
   a. Electric fields are about half, but B_1 homogeneity is much worse.
   b. Electric fields are lower by a factor of four, and B_1 homogeneity is much better.
   c. Sample heating is much lower; power handling and Q_L are much higher.
   d. Loaded Q and filling factor are higher, but B_1 homogeneity is much worse.
8. Which of the following is not likely to produce a change in tuning or Q from rf heating during a high power decoupling pulse?
   a. A Cu coil of 0.05 mm foil mounted on quartz.
   b. Standard, high-power rf capacitors.
   c. A 0.15 mm Cu-CuNi-Cu sandwich foil on silicon nitride.
   d. A zirconia stator.
   e. The sample.
9. The $\mathbf{B}_0$ perturbations from chip capacitors very close to the sample in MAS may be minimized by mounting them
   a. In a circle, equally spaced around the axis.
   b. Such that the angle between each capacitor and the nearest portion of the sample is $\sim 55°$ with respect to $\mathbf{B}_0$.
   c. With heavy, diamagnetic leads to compensate the capacitor's paramagnetism.
   d. All of the above.
10. Tuning stability of the proton coil in an H-X VAS probe at high fields requires
    a. A single-tuned, low-inductance, proton coil.
    b. The proton coil tuned very close to the proton frequency when the leads are detached.
    c. A low-impedance transmission line for the proton coil leads.
    d. All of the above.
    3. Only a and b are true.

11. Disadvantages of silicon nitride stators include
    a. Inferior wear resistance.
    b. Short T_1 of the silicon signal.
    c. Incompatibility with zirconia rotors at extreme temperatures.
    d. Poor thermal conductivity.
    e. All of the above.

REFERENCES

1. R. Andrew, "Magic Angle Spinning," In: *Encyclopedia of NMR*, D. M. Grant and R. R. Harris, Eds., Vol. 5, Wiley, 1996, pp. 2891–2900.
2. D. Burum, "Cross Polarization in Solids," In: *Encyclopedia of NMR*, D. M. Grant and R. R. Harris, Eds., Vol. 3, Wiley, 1996, pp. 1535–1542.
3. P. A. Keifer, L. Baltusis, D. M. Rice, A. A. Tymiak, and J. N. Shoolery, "A Comparison of NMR Spectra Obtained for Solid-Phase-Synthesis Resins Using Conventional High-Resolution, MAS, and HR-MAS Probes," *J. Magn. Reson. A*, **1996**, *119*, 65–75.
4. V. W. Miner and W. W. Conover, "Shimming of Superconducting Magnets," In: *Encyclopedia of NMR*, D. M. Grant and R. R. Harris, Eds., Vol. 7, Wiley, 1996, pp. 4340–4356.
5. T. M. Barbara, "Cylindrical Demagnetization Fields and Microprobe Design in High-Resolution NMR," *J. Magn. Reson. A*, **1994**, *109*, 265–269.
6. F. D. Doty, "NMR MAS Sealing Sample Cells and Methods" (patent pending).
7. I. D. Gay, "A Magic-Angle Spinner for Vacuum-Sealed Samples,' *J. Magn. Reson.*, **1984**, *58*, 413–420.
8. F. D. Doty and P. D. Ellis, "Design of High Speed Cylindrical NMR Sample Spinners," *Rev. Sci. Instrum.*, **1981**, *52*, 1868–1875.
9. V. J. Bartuska and G. E. Maciel, "A Magic-Angle Spinning System for Bullet-Type Rotors in Electromagnets," *J. Magn. Reson.*, **1981**, *42*, 312.
10. J. W. Beams, "Centrifuge," In: *The Encyclopedia of Physics*, R. M. Besancon, Ed., 2nd ed., Van Nostrand Reinhold, NY, 1974, pp. 123–126.
11. F. D. Doty and G. Entzminger, "Thermal Gradients and Centrifugation in HR MAS," presented at the 39th Rocky Mountain Analytical Conference, Denver, 1997.
12. M. J. E. Golay and N. J. Rumson, "Nuclear Magnetic Resonance Apparatus," U.S. Pat. No. 3,569,823, 1971.
13. P. Starewicz, Resonance Research, Inc., personal communication, 1996.
14. A. Sodickson and D. G. Cory, "Shimming a High-Resolution MAS Probe," *J. Magn. Reson.*, **1997**, *128*, 87–91.
15. D. I. Hoult and R. Deslauriers, "Accurate Shim-Coil Design and Magnet-Field Profiling by a Power-Minimization-Matrix Method," *J. Magn. Reson. A*, **1994**, *108*, 9–20.
16. L. F. Fuks, F. S. C. Huang, C. M. Carter, W. A. Edlstein, and P. B. Roemer, "Susceptibility, Lineshape, and Shimming in High-Resolution," *J. Magn. Reson.*, **1992**, *100*, 229–242.
17. A. D. Bax, "A Spatially Selective Composite 90° RF Pulse," *J. Magn. Reson.*, **1985**, *65*, 142–145.
18. S. N. Sarkar, H. W. Dodgen, and J. P. Hunt, "Multinuclear MR Frequency Shifts of Hydrated Ions as a Function of Applied Pressure and Temperature," *J. Magn. Reson. B*, **1996**, *112*, 197–199.
19. A. Bielecki and D. P. Burum, "Temperature Dependence of ^{207}Pb MAS Spectra of Solid Lead Nitrate: An Accurate, Sensitive Thermometer for VT MAS," *J. Magn. Reson. A*, **1995**, *116*, 215–220.
20. A. Allerhand and S. R. Maple, "Requirements for Ultrahigh Resolution NMR of Large Molecules on High-Field Instruments," *J. Magn. Reson.*, **1988**, *76*, 375–379.
21. D. W. Alderman and D. M. Grant, "An Efficient Decoupler Coil Design Which Reduces Heating in Conductive Samples in Superconducting Spectrometers," *J. Mag. Reson.*, **1979**, *36*, 447–451.
22. F. D. Doty, "Solid State Probe Design," In: *Encyclopedia of NMR*, D. M. Grant and R. R. Harris, Eds., Vol. 7, Wiley, New York, 1996, pp. 4475–4484.
23. D. L. VanderHart, "Magnetic Susceptibility and HR NMR in Liquids and Solids," In: *Encyclopedia of NMR*, D. M. Grant and R. R. Harris, Eds., Vol. 5, Wiley, New York, 1996, pp. 2938–2945.
24. F. D. Doty, Y. A. Yang, and G. E. Entzminger, "Magnetism in NMR Probe Design: Part I: General Methods," *Concepts Magn. Resn.*, **1998**, *10*, 133–156.
25. B. Gerstein, "CRAMPS," In: *Encyclopedia of NMR*, D. M. Grant and R. R. Harris, Eds., Vol. 3, Wiley, New York, 1996, pp. 1501–1508.
26. X. Wu and K. Zilm, "Cross Polarization with High-Speed MAS," *J. Magn. Reson. A*, **1993**, *104*, 154–163.
27. D. I. Hoult, "The NMR Receiver: A Description and Analysis of Design," *Prog. NMR Spectrosc.*, **1978**, *12*, 41.
28. G. J. Kost, S. E. Anderson, G. B. Matson, and C. B. Conboy, "A Cylindrical-Window NMR Probe with Extended Tuning Range for Studies of the Developing Heart," *J. Magn. Reson.*, **1989**, *82*, 238–252.
29. F. D. Doty, "Probe Design and Construction," In: *Encyclopedia of NMR*, D. M. Grant and R. R. Harris, Eds., Vol. 6, Wiley, New York, 1996, pp. 3753–3761.
30. D. M. Ginsberg and M. J. Melchner, "Optimum Geometry of Saddle Shaped Coils for Generating a Uniform Magnetic Field," *Rev. Sci. Instrum.*, **1970**, *41*, 122–123.

31. F. D. Doty and Y. Yang, "HR MAS NMR Coils with Magic Angle Capacitors" (patent pending).
32. Y.-Y. Lin, P. Hodgkinson, M. Ernst, and A. Pines, "A Novel Detection-Estimation Scheme for Noisy NMR Signals: Applications to Delayed Acquisition Data," *J. Magn. Reson.*, **1997**, *128*, 30–41.
33. F. D. Doty, "Low Inductance Transverse Litz Foil Coils," PCT WO 97/26560, 1997.
34. J. Adlerborn, M. Burstrom, L. Hermansson, and H. T. Larker, "Development of High Temperature High Strength Silicon Nitride By Glass Encapsulated Hot Isostatic Pressing," *Materials Design*, **1987**, *8*, 229–232.

F. David Doty obtained his Ph.D. in Physics at the University of South Carolina in 1983, where he worked on ESR instrumentation under C. Poole and H. Farach and on NMR instrumentation development under Paul Ellis. He and his wife Judy founded Doty Scientific, Inc., in 1982, in Columbia, South Carolina, where he continues as President and General Manager of Technology Development. He has over 20 publications and 25 patents in the areas of rf electronics, NMR probe technology, electromagnetism, manufacturing, turbomachinery, energy conversion cycles, ceramics, and acoustics. While his professional responsibilities keep him busy nearly 200% of the time, he still finds time to hike in the mountains or along the beach and to sing regularly with the church choir. His specific development projects constantly change with the interests of NMR customers.

George Entzminger, Jr., has worked as an electrical engineer with Doty Scientific, Inc., since 1986 immediately after receiving his B.S. in Electrical Engineering from the University of South Carolina. He is presently company Vice President and Service Manager for Doty and performs and evaluates many of the NMR probe development experiments. He has been doing hands-on work with NMR probes and techniques for the last 11 years. His work and ideas directly contributed to many of the features of the XC5 HR MAS probe.

Y. Andy Yang received his Ph.D. in physics from the University of Virginia in 1991, under the supervision of Louis Bloomfield. His graduate research involved the study of molecular clusters by means of mass spectroscopy and photoelectron spectroscopy. He joined Doty Scientific, Inc., in 1994. His current focus is on solving probe rf electronics problems and customer support. His current research interests include rf and magnetism modeling of NMR probes.